Ceria-Based Solid Electrolytes for IT-SOFC Applications

A. Arabaci*

Istanbul University-Cerrahpasa, Engineering Faculty, Department of Metallurgical and Materials Eng.,
34320 Avcilar-Istanbul/Turkey

In this study, doped ceria solid electrolyte materials $Ce_{0.8}M_{0.2}O_{2-\delta}$ (M = Gd, Sm, and Nd) for intermediate temperature-solid oxide fuel cells were synthesized through citrate-nitrate auto combustion method. They were then characterized by X-ray diffraction (XRD), scanning electron microscope (SEM), and Fourier transform infrared (FT-IR) techniques. XRD results show that all the synthesized powders indicate a single-phase with cubic fluorite structure. Electrolytes with high density were obtained by sintering the samples at 1400 °C for 6 h. The mean crystallite sizes were calculated using the Scherrer formula. Surface morphologies of all the sintered electrolytes were obtained by using SEM. The total ionic conductivity of all electrolytes was measured from the impedance analysis in 300–700 °C temperature range. The ionic conductivities at 700 °C are in the order of $Ce_{0.8}Sm_{0.2}O_{2-\delta}$ >$Ce_{0.8}Gd_{0.2}O_{2-\delta}$ >$Ce_{0.8}Nd_{0.2}O_{2-\delta}$, and their corresponding activation energies are found to be 0.61, 0.62, and 0.67 eV, respectively.

1. Introduction

Ceria is a main component of a solid oxide electrolyte. A solid electrolyte as an oxide ion conductor is the main component of a solid-oxide fuel cell (SOFC) which can be considered as a promising device due to its high efficiency and environmental friendly nature [1–5]. The electrolyte material is sandwiched between the cathodes and anodes. At high temperatures, zirconium oxide-based materials are commonly used as solid oxide electrolytes in SOFC applications. This is because of their excellent ionic conductivity, high chemical and mechanical stability. However, high operating temperatures induce high costs, differences in thermal expansion coefficients and lead to reactions between the cell components [6]. As mentioned before, solid oxide ion electrolyte material plays a crucial role based on IT-SOFC. Therefore, it is required to reduce the operating temperature and develop novel solid oxide ion conductors for the intermediate temperature range (500–700 °C) to advance the SOFC technology.

Fluorite structured ceria doped with rare earth has been revealed to be a promising electrolyte material for IT-SOFCs operating at < 700 °C [7, 8]. Ceria doped with gadolinia and ceria doped with samarium have been reported to possess the highest ionic conductivity [9], among the other rare earth elements doped ceria. On the other hand, Kamiya et al. reported that the oxygen diffusion co-efficient of ceria doped with Nd is larger than that of ceria doped with Gd, and many other rare earth elements with the same amount.

If cubic flourite ceria is doped with alkaline earth and rare earth oxides, oxygen vacancy is introduced in

the host lattice to maintain the charge balance. The defect reaction can be described in Kröger-Vink notation as given below for addition of M (M = Gd, Sm, Nd) in the ceria matrix,

$$M_2O_3 \xrightarrow{2CeO_2} 2M'_{Ce} + 3O^x_o + V^{\bullet\bullet}_o, \tag{1}$$
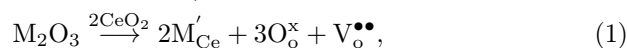
where M'_{Ce} shows one Ce^{4+} site that is replaced with M^{3+} ion. In fact, undoped ceria is a poor ionic conductor. When ceria is doped with rare earth cations, it may cause an increase in the oxygen vacancies which results in the increase of the ionic conductivity of CeO_2 to keep the charge balance.

In doped ceria with the fluorite type structure, the ionic conduction is realized via an oxygen vacancy diffusion mechanism. Oxygen ions' diffusion within the fluorite structure can be described as an thermally activated process with characteristic activation energy.

The ionic conductivity properties of the doped ceria can be significantly influenced by the type and amount of the dopant elements, sintering temperature, and the synthesis method. Also, the ionic conductivity of doped ceria is appreciably affected by the microstructure features such as the grain size [10].

Synthesizing ultrafine doped ceria powder is crucial to achieve dense electrolyte materials by sintering. According to the literature, doped cerium dioxide powders can be produced with a variety of techniques such as sol gel method, hydrothermal, coprecipitation, and combustion [11–13]. These reported processes are capable of synthesizing ultra-fine powders with narrow size distributions. Combustion synthesis is a wet chemical process that provides the possibility of obtaining ultra-fine doped cerium oxide powders with superior compositional homogeneity and easy controllability [14, 15].

The main advantages of this process are fewer stages and better control of stoichiometry while producing powders in the nanometer range. Citric acid, which

---

*e-mail: aliye@istanbul.edu.tr

is more cost-effective than the other organic fuels, acts as a complexing agent for a number of metal ions as it possess three carboxyl groups and one hydroxyl group. On the other hand, citric acid can also serve as fuel in the combustion reaction.

In this paper, Gd^{3+}, Sm^{3+}, and Nd^{3+} rare earth ions are used as dopants. Dopant amount was fixed at 20%. Doped ceria-based $Ce_{0.8}M_{0.2}$ (M = Gd, Sm, Nd) $O_{2-\delta}$, materials were prepared by the citrate-complexation method, and characterized. Effects of the rare earth elements on CeO_2 are investigated by studying their structure with XRD, microstructure with SEM, and ionic conductivity with impedance spectroscopy. In order to enhance the performance of the solid oxide fuel cells for intermediate-temperature applications, such as rare earth ions Gd^{3+}, Sm^{3+}, and Nd^{3+}, are more suitable as dopant ions.

2. Materials and method

$Ce_{0.8}Sm_{0.2}O_{1.90}$ (SDC), $Ce_{0.8}Gd_{0.2}O_{1.90}$ (GDC), and $Ce_{0.8}Nd_{0.2}O_{1.90}$ (NDC) samples were synthesized by using the low temperature citrate-complexation method as described in our previous work [16]. Cerium nitrate salt $(Ce(NO_3)_3 \cdot 6H_2O$, Aldrich, 99.99%), gadolinium nitrate salt $(Gd(NO_3)_3 \cdot 6H_2O$, Aldrich, 99.99%), neodymium $(Nd(NO_3)_3 \cdot 6H_2O$, Aldrich, 99.9%), and anhydrous $C_6H_8O_7$ were used as starting materials. The molar ratio of the cations to citric acid was 1:1.

To produce the SDC, GDC, NDC electrolyte samples, calculated amounts of metal salts were dissolved in deionized water to acquire a transparent solution. Then, anhydrous citric acid was added into the solution at 1:1 molar ratio with the cations, as a chelating agent and fuel, as well. These solutions were constantly stirred for approximately 30 min with a magnetic stirrer The solution was heated up to 85 °C utilizing a hot plate until the yellowish gel was obtained. After that, the gel was dried in an oven. The dried gel was heated in a furnace at 300 °C for 2 h under air atmosphere and self-ignited until the yellow powders were produced. The generated yellow powders were calcined at 600 °C to achieve powders without carbonaceous elements.

The synthesized powders were calcined at 600 °C for 3 h to remove the carbon residues and form a well crystalline fuorite structure. Then the powders were pressed with a hydraulic press under 50 N/mm^2 to prepare green pellets with 10 mm diameter and 1.5 mm thickness. Then, the pellets were sintered at 1400 °C for 6 h. After that, these disc-shaped pellets were pressed by cold isostatic press under 200 N/mm^2. Finally, the obtained pellets were sintered at 1400 °C for 6 h with 5 °C/min heating rate. Density values of the sintered solid oxide pellets were measured considering the Archimedes' principle and were estimated to be > 90% of theoretical density.

X-ray diffraction measurements were conducted with a D/max-2200 ultima X-ray diffractometer (Rigaku) to check the phase purity and to determine the particle size

and lattice parameter of the solid oxide electrolyte samples. Diffraction data of the doped ceria particles were recorded in a 2θ range from 10° to 90°.

FT-IR analyses (with a Perkin Elmer Spectrrum 100 instrument) were carried out to study the structures of SDC, GDC, and NDC by using Potassium bromide pellet technique in the wave number range of 350–4000 cm^{-1}.

Microstructures of the combustion powders and surfaces of the sintered pellets were observed using the scanning electron microscopy (FEI QUANTA FEG 450 scanning electron microscope).

Ag paste was applied to the both faces of the sintered pellets to prepare the electrode for the conductivity analyses, and the whole structure annealed at 800 °C for 30 min. The conductivity measurements of the sintered M (M= Gd, Sm, Nd) doped cerium oxide pellets were performed in a tube furnace by using two probe methods in the air. AC impedance analyser SOLARTRON 1260 FRA was used to carry out the measurements in a frequency range of 10 MHz to 100 mHz. The ionic conductivity measurements of the sintered pellets were taken within 50 °C intervals in the temperature range of 300 °C to 800 °C in the air. Data were collected with SMART program and fitted to the corresponding equivalent circuits with the ZView Program. A complex plane plot of real impedance (Z') versus imaginary impedance (Z'') was prepared for each set of data.

Overall resistance of the electrolyte is given by

$$R_{\text{overall}} = R_{\text{g}} + R_{\text{gb}} \qquad (2)$$

where R_{overall} is the total resistance, R_{g} is the grain resistance, and R_{gb} represents the grain boundary resistance.

Then, the conductivity can be calculated with

$$\sigma = \frac{l}{S} R_{\text{overall}}, \qquad (3)$$

where l and S are the sample thickness and the area of the sample surface, respectively.

3. Results and discussions

3.1. Crystal structure

Figure 1 depicts the X-ray diffraction patterns of $Ce_{0.8}Sm_{0.2}O_{1.90}$, $Ce_{0.8}Gd_{0.2}O_{1.90}$, $Ce_{0.8}Nd_{0.2}O_{1.90}$ solid oxide electrolyte samples calcined at 600 °C for 3 h. All diffraction peaks are well indexed (JCPDS no. 34-0394) to the single phase with cubic fluorite structure. No additional phases corresponding to Gd_2O_3, Sm_2O_3, or Nd_2O_3 were observed which ensured the complete dissolution of the dopant elements in the cerium oxide lattice. The mean crystallite sizes calculated by using the Scherrer formula were 12, 17, and 19.2 nm for $Ce_{0.8}Sm_{0.2}O_{1.90}$, $Ce_{0.8}Gd_{0.2}O_{1.90}$, and $Ce_{0.8}Nd_{0.2}O_{1.90}$, respectively.

The introduction of Sm^{3+}, Gd^{3+}, and Nd^{3+} ions into Ce^{4+} can cause a small shift in the cerium oxide peaks positions. X-ray peaks shifted toward the higher 2θ value. This shift was attributed to the increase of the ionic diameter of Nd^{3+}(1.109 Å)>Sm^{3+}(1.079 Å)> Gd^{3+}(1.053 Å)>Ce^{4+}(0.970 Å). Figure 1 shows the shift
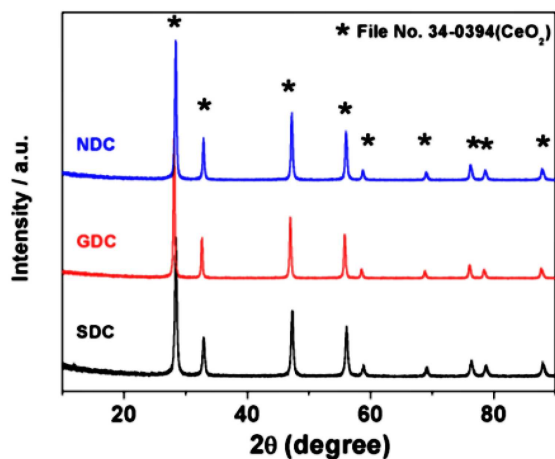
Fig. 1. XRD patterns of the calcined $Ce_{0.8}Sm_{0.2}O_{1.90}$(SDC), $Ce_{0.8}Gd_{0.2}O_{1.90}$(GDC), $Ce_{0.8}Nd_{0.2}O_{1.90}$(NDC) powders.

of the peaks. This shift can be attributed to the change in the lattice parameter. Lattice parameters of the SDC, GDC, and NDC samples were calculated to be 5.425 Å, 5.437 Å, and 5.447 Å, respectively.

3.2. Microstructure

The microstructure of the sintered pellets of $Ce_{0.8}M_{0.2}O_{1.90}$ (M = Sm, Gd, Nd) was studied by SEM. SEM micrographs of the outher surfaces of the sintered $Ce_{0.8}Sm_{0.2}O_{1.90}$, $Ce_{0.8}Gd_{0.2}O_{1.90}$, $Ce_{0.8}Nd_{0.2}O_{1.90}$ electrolyte samples are given in Fig. 2. It can be observed that NDC, GDC, and SDC samples are all well sintered. There are no pores recognized on the sample surfaces, which are consistent with the measured density of the sintered pellets. The sintered pellets have a relative density of 95%. The average grain size of each sample was found to be in the range of 0.67–0.78 μm.

3.3. Fourier transform infrared (FTIR) spectroscopy

Fourier transform infrared (FTIR) spectra of the calcined SDC, GDC, and NDC powders are shown in Fig. 3. There are some distinctive absorptions peaks at 3430 and 1628 cm^{-1}. In addition, some weaker absorption peaks were also observed at around 2930, 1092, and 700 cm^{-1}.

The strong band at 3430 cm^{-1} is attributed to the ν(O–H) vibration modes of the physically adsorbed water molecules. The less intense peaks at 2930 cm^{-1} are attributed to the stretching vibration of the CH_2 group. Absorption at 1628 cm^{-1} is assigned to a systematic stretching vibration of the COO^- group [17]. The peak at around 1090 cm^{-1} indicates the presence of the nitrate ions [18]. The bands observed in the lower frequency region at 700 and 430 cm^{-1} are referred to the characteristic Ce–O vibration [19]. Although the presence of the COO^- group and nitrate ions, a dense structure was obtained after sintering, as seen in Fig. 2.
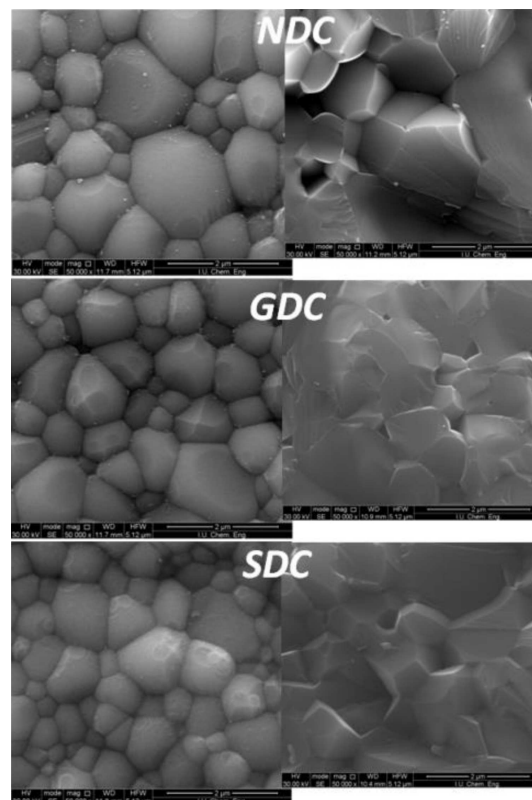
Fig. 2. SEM micrographs of SDC, GDC and NDC samples sintered at 1400 °C in the air.

3.4. Impedance results

Electrical Impedance Spectroscopy (EIS) is a useful device to understand the electrical features of polycrystalline solid oxide electrolytes. EIS makes it possible to obtain information about the fuel cell system, i.e. anode, cathode, and the electrolyte. In Fig. 4a, contributions of three separate semi-circles are recognized. These semicircles belong to the grain, grain boundary, and electrode resistances, respectively, from left to right. At such a low operating temperature, i.e., 300 °C, three arcs can be observed in the Nyquist plot. However, as the operating temperature increases, the semicircle that corresponds to the grain resistivity disappears and only the grain and electrode resistivity are observed at 400–500 °C. Bulk resistivity could be calculated by measuring the distance between the origin and the starting point of the grain boundary semicircle. Beyond 500 °C, only the semicircle that represents the electrode remains and it is impossible to determine the bulk or grain resistivity separately. Therefore, only the total resistivity could be calculated at temperatures higher than 500 °C. The real axis intercept of high frequency arc delineates the grain resistance and intercept of intermediate frequency arc defines the grain boundary resistance. The total resistance is the sum of these two resistances. The total resistance of the electrolyte is given by (2), and the overall conductivity can be found using (3).
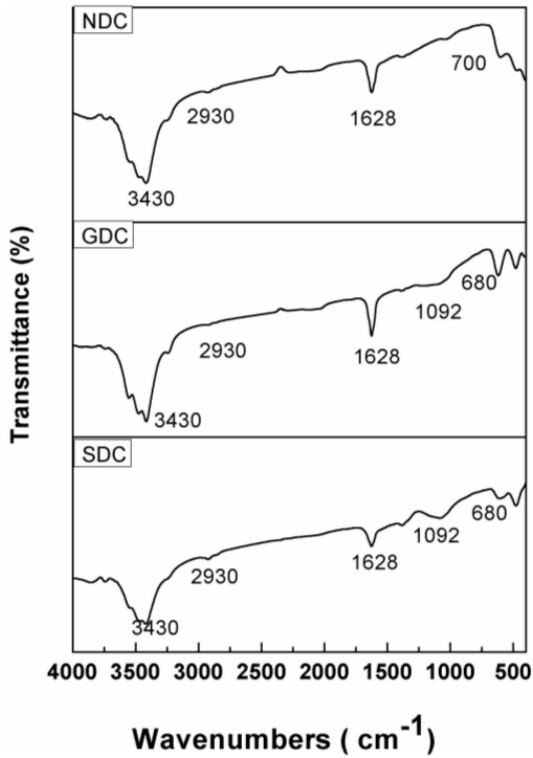
Fig. 3. FTIR spectra of the calcined $Ce_{0.8}M_{0.2}O_{1.90}$ powders (M= Sm, Gd, Nd).

Fig. 4. (a) The impedance spectrum of SDC at 300 °C, the impedance spectrum of SDC, GDC and NDC samples (b) at 400, and (c) 700 °C.
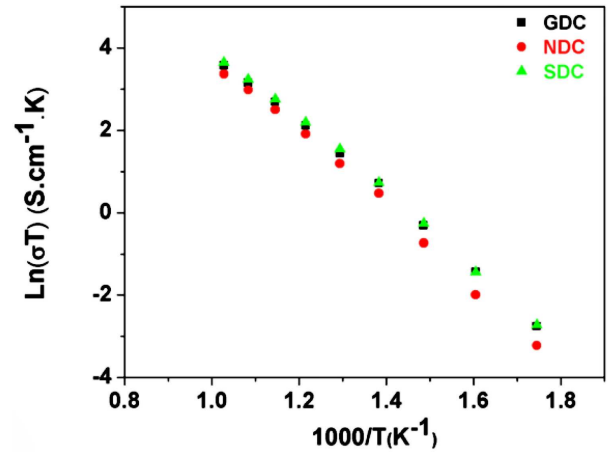
Fig. 5. Total electrical conductivity obtained for $Ce_{0.8}M_{0.2}O_{1.90}$ (M= Sm, Gd, Nd) electrolyte sintered at 1400 °C.

Figures 4b and 4c show that the both grain and grain boundary resistance decrease with the increasing operating temperature. The decrease in the grain boundary resistance with the increasing temperature may arise from the lowering of the barrier that favors the increase of mobility of the charge carriers [20].

Activation energies E, which are the sum of the association energy E_a and the migration energy E_m, were calculated by fitting the conductivity data to the Arrhenius relation for thermally activated conduction. This relation is given by

$$\sigma = \frac{\sigma_0}{T} \exp\left(-\frac{E}{k_B T}\right), \qquad (3)$$

where σ_0 is a pre-exponential factor being a constant in a certain temperature range, T is the absolute temperature, k_B represents the Boltzman's constant, and E is the activation energy of electrical conduction. This energy E can be calculated from the slope of the Arrhenius plot. Figure 5 shows for all $Ce_{0.8}M_{0.2}O_{2-\delta}$ (M= Sm, Gd, Nd) samples that the conductivity values increase with temperature.

In Fig. 5, the Arrhenius plot of $Ce_{0.8}M_{0.2}O_{1.90}$, doping with the Sm and Gd cations mentioned above, improved the total conductivity compared to cerium oxide doped with Nd cation. Among the current doping cations in this study, Sm^{3+} gave the best results ($\sigma_{Total} = 2.77 \times 10^{-2}$ S/cm at intermediate temperature of 650 °C with $E = 0.61$ eV). This conductivity value is higher than the reported conductivity values of $Ce_{0.85}Sm_{0.15}O_{2-\delta}$ (MS-SDC) (1.44×10^{-2} S/cm), $Ce_{0.85}La_{0.15}O_{2-\delta}$ (MS-LDC) (1.30×10^{-2} S/cm) [20], and $Ce_{0.80}Gd_{0.20}O_{1.90}$ (1.29×10^{-2} S/cm) [19] at 650 °C. Conductivity of $Ce_{0.8}Sm_{0.2}O_{1.90}$ was nearly two times that of $Ce_{0.85}Sm_{0.15}O_{2-\delta}$ (MS-SDC), $Ce_{0.85}La_{0.15}O_{2-\delta}$ (MS-LDC), and $Ce_{0.80}Gd_{0.20}O_{1.90}$.

The slope of the conductivity curve in Fig. 5 also shows that a bending occurs at 500–550 °C for almost all samples, which is interpreted as a transition from associated to disassociated behavior in defect clusters, and consequently as a decrease in the activation energy [10]. Moreover, this situation implies that the conduction mechanism changes at a transition temperature. Thus, there are two different conduction mechanisms at different operating temperature regimes. According to the Arrhenius

plots (in Fig. 5), there are two parts named as low temperature (LT) and high temperature (HT) regimes in which the linearity of the Arrhenius plots change. The activation energy for conduction becomes the sum of activation energy for migration E_m and association E_a ($E = E_m + E_a$). It can be said that at high temperature regimes, the dopant-oxygen vacancy complex dissociates completely to set free the dopant cations and oxygen vacancy. The oxygen vacancy concentration is known to not depend on temperature and is equivalent to the total concentration of dopant cations. Therefore, the migration enthalpy can be calculated from the slope of Arrhenius plots in the higher temperature regime. A similar behaviour was also observed in earlier studies [21, 23].

4. Conclusion

Rare earth doped $Ce_{0.8}M_{0.2}O_{1.90}$ (M= Gd, Nd, Sm) solid solutions with the fluorite structure were prepared by the citrate-complexation method. The rare earth (M = Gd, Nd, Sm) doped ceria particles reveal the cubic fluorite structure of pristine CeO_2 with small lattice strains. Dense solid oxide electrolytes were obtained by sintering the pellets at $1400\,°C$ for 6 h. The relative densities were over 90% of the theoretical density and these results are consistent with the SEM studies. In accordance with the results of ionic conductivity the highest ionic conductivity value was calculated as 2.77×10^{-2} S/cm at $650\,°C$ for SDC. This value is 31.9% higher than NDC (2.1×10^{-2} S/cm) and 10.8% higher than GDC (2.5×10^{-2} S/cm) at intermediate temperature of $650\,°C$. It can be concluded that the current conductivity values make $Ce_{0.8}Sm_{0.2}O_{1.90}$ a potential candidate material to be used as a solid electrolyte in IT-SOFCs.

Acknowledgments

References

[1] B.C.H. Steele, *Solid State Ionics* **129**, 95 (2000).

[2] S.P.S. Badwal, K. Foger, *Ceram. Int.* **22**, 257 (1996).

[3] A. Arabacı, *Emerg. Mater. Res.* **9**, 1 (2020).

[4] B. Madhavan, A.K. Kunhiraman, V. Ragavi, *Emerg. Mater. Res.* **9**, 1 (2020).

[5] M. Cengiz Toklu, H. Taşkın, *IJCESEN* **4**, 6 (2018).

[6] H. Inaba, H. Tagawa, *Solid State Ionics* **83**, 1 (1996).

[7] G.B. Jung, T.J. Huang, M.H. Huang, C.L. Chang, *J. Mater. Sci.* **36**, 5839 (2001).

[8] T. Mori, J. Drennan, J.H. Lee, J.G. Li, T. Ikegami, *Solid State Ionics* **154**, 461 (2002).

[9] H. Yahiro, Y. Eguchi, K. Eguchi, H. Arai, *J. Appl. Electro-Chem.* **185**, 909 (1988).

[10] D.R. Ou, T. Mori, F. Ye, J. Zou, J. Drennan, *Renew. Energy* **33**, 197 (2008).

[11] M. Guo, J. Lu, Y. Wu, Y. Wang, M. Luo, *Langmuir.* **27(7)**, 3872-7 (2011).

[12] S. Zha, C. Xiang. G. Meng, *J. Power Sources* **115**, 44 (2003).

[13] R.D. Purohit, B.P. Sharma, K.T. Pillai, A.K. Tyagi, *Mater. Res. Bull.* **36**, 2711 (2001).

[14] T. Mahata, G. Das, R.K. Mishra, B.P. Sharma, *J. Alloys Compd.* **391**, 129 (2005).

[15] H. Xu, H.Yan, Z.Chen, *J. Power Sources* **163**, 409 (2006).

[16] A. Arabacı, *Solid State Ionics* **326**, 69 (2018).

[17] S. Shrestha, C.M.Y. Yeung, C. Nunnerley, S.C. Tsang, *Sens. Actuators A* **A136**, 191 (2007).

[18] J. Tartaj, V. Gil, A. Moure, *J. Power Sources* **195**, 2800 (2010).

[19] N. Shehata, K. Meehan, M. Hudit, N. Jain, *J. Nanopart. Res.* **14**, 1173 (2012).

[20] T. Badapanda, V. Senthil, S.K. Raut, S. Panigrahi, T.P. Sinha, *Mat. Chem. Phys.* **133**, 863 (2012).

[21] M. Gupta, S. Shirbhate, P. Ojha, S. Acharya, *Solid State Ionics* **320**, 199 (2018).

[22] Y.P. Fu, S.H. Chen, J.J. Huang, *Int. J. Hydrog. Energy* **35**, 745 (2010).

[23] J.S. Kilner, C.D. Waters, *Solid State Ionics* **6**, 253 (1982).